frontiers in Built Environment

ORIGINAL RESEARCH
published: 15 March 2021
doi: 10.3389/fbuil.2021.656606

Optimal Seismic Design of Stiffness and Gap of Hysteretic-Viscous Hybrid Damper System in Nonlinear Building Frames for Simultaneous Reduction of Interstory Drift and Acceleration

*Soichiro Ishida and Izuru Takewaki**

Department of Architecture and Architectural Engineering, Graduate School of Engineering, Kyoto University, Kyoto, Japan

OPEN ACCESS

Edited by:
Solomon Tesfamariam, University of British Columbia Okanagan, Canada

Reviewed by:
Said Elias Rahimi, University of Iceland, Iceland
Michele Palermo, University of Bologna, Italy

****Correspondence:***
Izuru Takewaki
takewaki@archi.kyoto-u.ac.jp

Specialty section:
This article was submitted to Earthquake Engineering, a section of the journal Frontiers in Built Environment

Received: *21 January 2021*
Accepted: *11 February 2021*
Published: *15 March 2021*

Citation:
Ishida S and Takewaki I (2021) Optimal Seismic Design of Stiffness and Gap of Hysteretic-Viscous Hybrid Damper System in Nonlinear Building Frames for Simultaneous Reduction of Interstory Drift and Acceleration. Front. Built Environ. 7:656606. doi: 10.3389/fbuil.2021.656606

The viscous-hysteretic hybrid (HVH) damper system recently introduced by one of the authors has a clear property that, when the hysteretic dampers with gap mechanism become active (stiffness element starts working), the acceleration of building frames with this damper system as a stopper attains large values in spite of the advantageous feature to prevent excessive deformation. It is therefore desired that both the maximum interstory drift and the maximum acceleration exhibit an acceptable value with appropriate compromise. The double impulse as a simplified version of one-cycle sine wave as a representative of the main part of near-fault ground motions can simulate the maximum interstory drifts properly. However, it cannot simulate the maximum accelerations due to its impulsive nature. In this case, the sine wave corresponding to the double impulse can play an important role in the reliable simulation of the maximum accelerations. Even in such circumstance, the analysis using the double impulse is important because it enables to obtain the critical timing of the input, i.e. the nonlinear resonant frequency of the sine wave without repetition. The investigations on the criticality of the sine wave corresponding to the critical double impulse show that the critical timing of the double impulse leads to the nonlinear resonant frequency of the sine wave in view of the maximum interstory drift, the maximum top acceleration and the maximum relative acceleration for the constant input acceleration and the constant input velocity except for some cases. It is demonstrated finally that the index in terms of the maximum interstory drift and the maximum acceleration can be introduced as an appropriate parameter for deriving the optimally compromised gap quantity of hysteretic dampers with gap mechanism for various input velocity levels and various hysteretic damper stiffness ratios.

Keywords: tall building, hysteretic damper, gap mechanism, double impulse, deformation-acceleration control, stopper mechanism

INTRODUCTION

Recently, "resilience" is becoming a principal target of structural and infrastructural design in the world that faces rapidly-changing natural hazard risks. Various methods and strategies have been proposed for upgrading the resilience performance from several different viewpoints. Bruneau et al. (2003) introduced the concept of resilience in the field of structural engineering for the first time and provided the so-called "resilience triangle". Cimellaro et al. (2010) quantified the resilience in the framework of the resilience triangle. Takewaki et al. (2011) explained the significance and effectiveness of structural control in the upgrade of the resilience. Noroozinejad et al. (2019) focused on the review of the concept of resilience in the structural and infrastructural engineering. In the usual framework, the resistance to risks and the recovery from damaged states after disturbances are defined as two main phases in the resilience. The past history in the structural and infrastructural design indicated that, while the resistance has been treated as a main research field, the recovery has never been tackled satisfactorily due to various complicated factors related to multidisciplinary fields.

In place of the structural design philosophy to withstand earthquake and wind disturbances by the reasonable proportioning of member stiffness and strength, structural control has been introduced worldwide. The overall advances of structural control in each period are summarized in the literatures. Hanson (1993) and Aiken et al. (1993) pointed out the importance of introducing passive dampers in the structural design of buildings. Soong and Dargush (1997) and Hanson and Soong (2001) explained the properties of passive dampers and summarized the state of the arts up until around 2000. Takewaki (2009) and Lagaros et al. (2013) presented several design methods of passive dampers and summarized the development up until around 2010. After sufficient development of various passive damper systems, smart and optimal design (quantity and location) of passive dampers is becoming one of the main topics in the field of structural control. Various approaches to the design of linear and nonlinear viscous dampers have been developed. Aydin et al. (2007) extended the transfer function amplitude approach in terms of interstory drifts due to Takewaki (1997) (the unified formulation is shown in Takewaki (2009)) to base shears. Attard (2007) developed a gradient-based optimization algorithm for highly nonlinear degrading steel frames. Lavan and Levy (2010) presented another gradient-based method of optimal seismic retrofitting for yielding plane frames with viscous dampers by using an optimal control theory. Adachi et al. (2013) devised a unique gradient-based sequential algorithm for determining the optimal nonlinear viscous damper location and quantity in linear building frames. Akehashi and Takewaki (2019) used the critical excitation approach for the optimal viscous damper placement in elastic-plastic shear building structures to consider input uncertainties. In particular, a complete survey on the research of viscous dampers can be found in the review paper (De Domenico et al., 2019). While viscous dampers are faced with a cost problem, hysteretic dampers, e.g. buckling-restrained braces, have often been employed in earthquake prone countries. At the same time, simultaneous use of various types of dampers has been sought.

As for damper design methods, some useful investigations were conducted. The followings are some examples. Silvestri et al. (2010) and Palermo et al. (2016); Palermo et al. (2017); Palermo et al. (2018) proposed a practical design method of linear and nonlinear viscous dampers for linear building frames. Their methods consist of five steps. Its design philosophy is based on the limit of the structural damages under severe earthquakes. A target response reduction factor is chosen first for satisfying the condition on the desired reduction of the peak structural response. The equivalent linear viscous damping coefficients for nonlinear dampers are computed by using effectively the properties of modal damping ratios as classically damped systems. Elias and Mastsagar (2019) dealt with nonlinear frame responses using multiple TMD optimization. Although single TMD is effective for the control of linear frames, multiple TMDs were devised for controlling nonlinear frame responses. De Domenico and Ricciardi (2019) investigated an optimization problem of nonlinear viscous dampers used in building frames. The nonlinear power law in the constitutive relation of the devices was introduced in the optimal design process. Tabara and De Domenico (2020) investigated the design of nonlinear viscous dampers. They transformed the nonlinear viscous dampers into the equivalent linear model and enabled the application of the response spectrum method in the seismic response evaluation for sophisticated damper design.

While linear viscous dampers have been treated in the framework of linear formulation, the design of hysteretic dampers necessitates distinct kinds of treatment due to their peculiar characteristics. Murakami et al. (2013) introduced a relaxed and stabilized sensitivity-based approach applicable to hysteretic dampers. Numerical optimization algorithms including time-history response analysis for response evaluation are needed for taking into account these peculiar characteristics in hysteretic dampers. The algorithm including time-history response analysis requires a tremendous amount of computational effort to disclose original properties of the optimal damper location and quantity. In comparison with such conventional approaches, an innovative design method was developed by Shiomi et al. (2016) for hysteretic dampers. In this method, an explicit expression was taken full advantage for the maximum elastic-plastic response of a single-degree-of-freedom (SDOF) system with hysteretic dampers under "the critical double impulse" as a representative of near-fault ground motions (Kojima and Takewaki 2015). Then a direct and simple optimization was implemented using this explicit expression. Subsequently, Shiomi et al. (2018) proposed a novel control system called a "dual hysteretic damper (DHD)" system and developed a sensitivity-based optimal design method of damper placement for multi-degree-of-freedom (MDOF) systems. Recently, Hashizume and Takewaki (2020a); Hashizume and Takewaki (2020b) proposed another new vibration control system called a "hysteretic viscous hybrid (HVH)" damper system by replacing the DSA (short-range hysteretic damper) in the DHD system by a viscous damper.

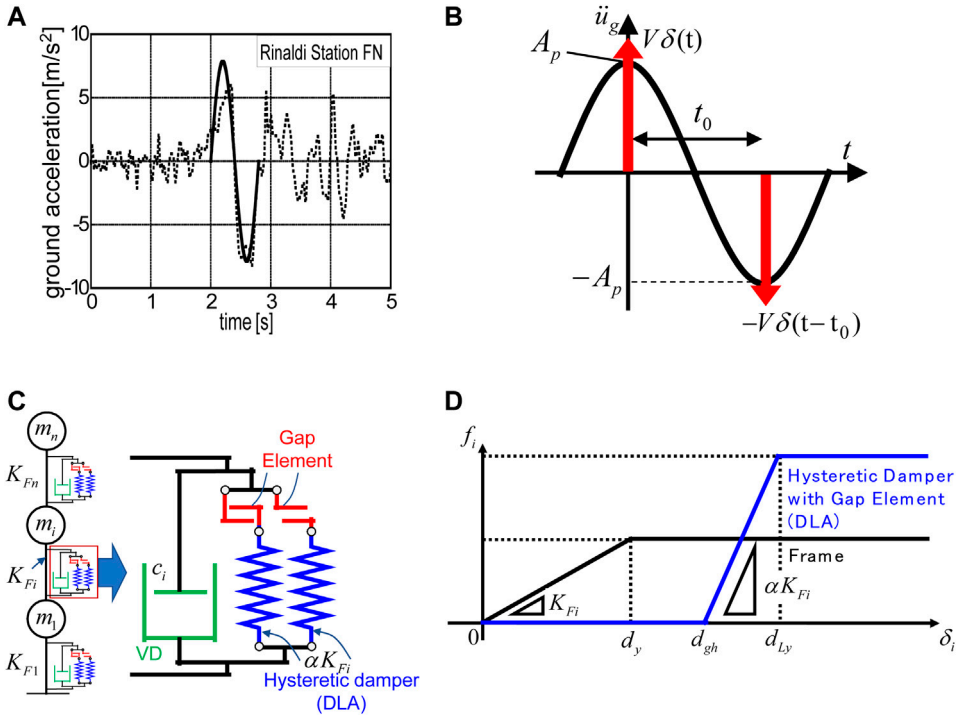

FIGURE 1 | Modeling of main part of ground motion into double impulse and passive control system HVH, **(A)** Transformation of main part of Rinaldi station FN motion (Northridge 1994) into one-cycle sine wave, **(B)** Transformation into double impulse, **(C)** Passive control system HVH, **(D)** Force-deformation relations of frame and hysteretic damper with gap mechanism (Partially from Shiomi et al., 2018 and Hashizume and Takewaki 2020b).

They clarified the response reduction performance of the DHD and the HVH for SDOF and MDOF systems.

In this paper, the HVH system introduced by Hashizume and Takewaki (2020a); Hashizume and Takewaki (2020b) will be investigated from two main viewpoints (stiffness and functionality). The stiffness can be measured in terms of the maximum interstory drift and the functionality (usability) can be evaluated in terms of the maximum acceleration. The HVH damper system consisting of viscous dampers and hysteretic dampers with gap mechanism has a clear property that, when the hysteretic dampers with gap mechanism become active (stiffness element starts working), the acceleration of building frames with this damper system as a stopper attains large values in spite of the advantageous feature to prevent excessive deformation. It is therefore desired that both the maximum interstory drift and the maximum acceleration exhibit an acceptable value with appropriate compromise. The double impulse as a simplified version of one-cycle sine wave as a representative of the main part of near-fault ground motions can simulate the maximum interstory drifts properly. However, it cannot simulate the maximum accelerations due to its impulsive nature. In this case, the sine wave corresponding to the double impulse can play an important role in the reliable simulation of the maximum accelerations. Even in such circumstance, the analysis using the double impulse is important because it can obtain the critical timing of the input, i.e. the nonlinear resonant input frequency of the sine wave without repetition. The investigations on the criticality of the sine wave corresponding to the critical double impulse show that the critical timing of the double impulse leads to the nonlinear resonant frequency of the sine wave in view of the maximum interstory drift except for some cases. A similar property on the criticality is also demonstrated for the maximum top acceleration and the maximum relative acceleration for the constant input acceleration and the constant input velocity. Finally, a new index in terms of the maximum interstory drift and the maximum acceleration is introduced as an appropriate parameter for deriving the optimally compromised gap quantity of hysteretic dampers with gap mechanism.

DOUBLE IMPULSE AS REPRESENTATIVE OF MAIN PART OF PULSE-TYPE GROUND MOTION

In the innovative energy approach by Kojima and Takewaki (2015), it was clarified that the property of the main part of a near-fault pulse-type ground motion can be captured by the double impulse. The double impulse has an advantage that it produces only a free-vibration component and the combination of free-vibration component and forced-vibration component is unnecessary. In this approach, the main part of a near-fault ground motion is first expressed by a one-cycle sine wave $\ddot{u}_{g\sin}(t)$ as shown in **Eq. 1** (see **Figure 1A**) and then put into a double impulse $\ddot{u}_g(t)$ expressed by **Eq. 2** (see **Figure 1B**).

$$\ddot{u}_{g\sin}(t) = A_p \sin \omega_p t, \tag{1}$$

$$\ddot{u}_g(t) = V\delta(t) - V\delta(t - t_0), \tag{2}$$

where A_p, ω_p, V, t_0 are the acceleration amplitude and circular frequency of the one-cycle sine wave, the velocity amplitude and time interval of the two impulses, respectively, and $\delta(t)$ is the Dirac delta function. The coincidence of the maximum Fourier amplitudes in this transformation was required to make their influences on the structural response equivalent. This transformation is explained in the following briefly (Akehashi et al., 2018).

The Fourier transform of **Eq. 2** can be expressed as

$$\ddot{U}_g(\omega) = V\left(1 - e^{-i\omega t_0}\right). \tag{3}$$

On the other hand, the Fourier transform of **Eq. 1** can be computed by

$$\ddot{U}_{g\sin}(\omega) = \int_0^{2t_0} \left\{A_p \sin\left(\omega_p t\right)\right\} e^{-i\omega t} \mathrm{d}t = \frac{\pi t_0 A_p}{\pi^2 - (\omega t_0)^2}\left(1 - e^{-2i\omega t_0}\right). \tag{4}$$

The Fourier amplitudes of both inputs are expressed by

$$\left|\ddot{U}_g(\omega)\right| = V\sqrt{2 - 2\cos(\omega t_0)}, \tag{5}$$

$$\left|\ddot{U}_{g\sin}(\omega)\right| = A_p\left|\frac{2\pi t_0 \sin(\omega t_0)}{\pi^2 - (\omega t_0)^2}\right|. \tag{6}$$

The ratio a of A_p to V as a principal index of this transformation is introduced by

$$A_p = aV. \tag{7}$$

The coefficient a as a function of t_0 can be derived as follows from **Eqs. 5**–**7** and the condition on equivalence of the maximum Fourier amplitude $\left|\ddot{U}_g(\omega)\right|_{\max} = \left|\ddot{U}_{g\sin}(\omega)\right|_{\max}$. Further investigation can be found in the references (Akehashi et al., 2018; Hashizume and Takewaki 2020b).

Consider the ratio of the maximum velocity V_p of the one-cycle sine wave to the velocity amplitude V of the double impulse. The velocity $\dot{u}_{g\sin}$ of the one-cycle acceleration sine wave is expressed by

$$\dot{u}_{g\sin}(t) = \int_0^t \ddot{u}_{g\sin}(t)\mathrm{d}t = \int_0^t A_p \sin\left(\omega_p t\right)\mathrm{d}t = \frac{A_p}{\omega_p}\left\{1 - \cos\left(\omega_p t\right)\right\}. \tag{8}$$

Eq.8 provides the maximum velocity V_p of the one-cycle sine wave.

$$V_p = \frac{2A_p}{\omega_p}. \tag{9}$$

Finally, based on the investigation after **Eq. 7** (Akehashi et al., 2018; Hashizume and Takewaki 2020b), V_p/V is expressed as

$$V_p \big/ V = 1.22\ldots \tag{10}$$

HYSTERETIC-VISCOUS HYBRID DAMPER SYSTEM AND RESPONSE OF FRAME WITH HVH UNDER DOUBLE IMPULSE AND CORRESPONDING SINE WAVE

Consider a hysteretic-viscous hybrid (HVH) damper system proposed in the recent papers (Hashizume and Takewaki, 2020a; Hashizume and Takewaki, 2020b). The most remarkable property of this damper system is to possess a gap mechanism in the hysteretic damper system and play a role as a stopper system. The gap mechanism gives the system a redundancy to the limit on the accumulated plastic deformation capacity. With this mechanism, the hysteretic damper with a gap mechanism exhibits a large-stroke performance.

A MDOF building structure including the HVH system is shown in **Figure 1C**. The building structure is modeled as a shear building model and the hysteretic damper is assumed to have the elastic-perfectly plastic restoring-force characteristics. Let K_{Fi}, α, c_i denote the frame stiffness in the i-th story, the stiffness ratio of the hysteretic damper (DLA) to the frame (constant through all stories) and the damping coefficient of the viscous damper in the i-th story. The fundamental natural period of the bare frame is 1.60 (s) as shown later and the story stiffness distribution of the bare frame is trapezoidal (the top to bottom story stiffness ratio = 0.5). It is assumed here that the damping coefficients of the viscous dampers are proportional to the elastic stiffnesses of the main frame. Let d_y, d_{gh}, d_{Ly} denote the yield interstory drift of the frame, the trigger displacement of DLA (gap quantity) and the yield displacement of DLA, respectively, (constant through all stories). In addition, f_i and δ_i denote the story shear force in the i-th story of the frame or hysteretic dampers and the interstory drift of the frame, respectively. The viscous damper is aimed at providing a restoring force for the broad-amplitude range vibration and the hysteretic damper with a gap mechanism is expected to play as a stopper for the large-amplitude range vibration.

The total story shear strength in the ith story can be expressed by $Q_{yi} = k_{Fi}d_y + \alpha k_{Fi}(d_{Ly} - d_{gh})$ and the corresponding yield shear force coefficient is expressed by $c_{yi} = Q_{yi}/\sum_{j=i}^{15} m_j g$ (m_j: jth story mass, g: acceleration of gravity). When $d_{Ly} - d_{gh} = d_y$, $Q_{yi} = (1 + \alpha)k_{Fi}d_y$. In addition, the strength ratio (ratio of the damper yield strength to the story yield strength of the entire system) is expressed by $\alpha k_{Fi}d_y/\{(1 + \alpha)k_{Fi}d_y\} = \alpha/(1 + \alpha)$.

In this section, the response reduction characteristic of the MDOF system with the HVH system is presented. Especially, the influence of DLA with gap mechanism as a stopper element will be investigated. The structural parameters of the main frame, the viscous damper and the hysteretic damper (DLA) in the MDOF system with the HVH system are shown in **Table 1**.

The nonlinear time-history response analysis was conducted by using a Newmark- β method (constant acceleration method). The accuracy of the analysis program was confirmed through the comparison with the general-purpose computer program, "SNAP" (SNAP 2015).

TABLE 1 | Structural parameters of main frame, viscous damper and hysteretic damper (HVH system).

Main frame			
Number of stories	Floor mass	Story height	Fundamental-mode damping ratio
15	4.0×10^5 (kg)	3.5 (m)	0.02
Story stiffness in first story	Frame yield interstory drift	Undamped fundamental natural period	Story stiffness distribution
7.2×10^8(N/m)	0.023 (m)	1.60 (s)	Trapezoidal (top to bottom stiffness ratio = 0.5)
DLA (hysteretic damper with gap mechanism)			**Viscous damper**
Hysteretic damper stiffness ratio α to frame	Trigger disp. of DLA (gap quantity)	Yield disp. of DLA	Damping ratio
0, 1, 2, 3	0.023 (m)	0.046 (m)	0.1

The critical timing of the second impulse can be obtained by conducting a time-history response analysis under the first impulse and identifying the time attaining the zero value of the story shear force in the first story (Akehashi and Takewaki, 2019).

The double impulse with the input velocity level $V = 2.0$ (m/s) is considered. The left figures in **Figure 2** show the time histories of the first, eighth and 15th-story interstory drifts of 15-story buildings with HVH system for various damper stiffness ratios $\alpha = 0, 1, 2, 3$ of hysteretic dampers under the critical double impulse and the corresponding sine wave expressed by **Eq. 1**. It can be observed that the double impulse can simulate the interstory drifts of a sine wave with the equivalent period. The right figures in **Figure 2** show the maximum interstory drift distributions for various damper stiffness ratios $\alpha = 0, 1, 2, 3$ of hysteretic dampers under the critical double impulse and the sine wave corresponding to the critical double impulse. It can be found that the double impulse can simulate the maximum interstory drift distributions of a sine wave with the equivalent period and the lower-story deformations can be well suppressed by increasing the hysteretic damper stiffness ratio.

Although the double impulse can simulate the maximum interstory drifts properly, it cannot simulate the maximum accelerations due to its impulsive nature. For this reason, the sine wave corresponding to the double impulse can play an important role in the simulation of the maximum accelerations. However, even in this case, the analysis using the double impulse is important in the sense that it enables to obtain the critical timing of the input, i.e. the nonlinear resonant frequency of the sine wave. This property will be discussed later in more detail.

INVESTIGATION ON NONLINEAR RESONANT FREQUENCY OF SINUSOIDAL WAVE TRANSFORMED FROM CRITICAL DOUBLE IMPULSE

In this section, the validity of the nonlinear resonant frequency of the sinusoidal wave transformed from the critical double impulse is investigated. The analysis using the double impulse is important because it enables to obtain the critical timing of the double impulse, i.e. the nonlinear resonant frequency of the sine wave without repetition. The investigations on the criticality of the sine wave corresponding to the critical double impulse are conducted in view of the maximum interstory drift, the maximum top acceleration and the maximum relative acceleration for the constant input acceleration and the constant input velocity except for some cases. **Eq. 9** is used for realizing the constant input acceleration and the constant input velocity.

Figure 3 shows the maximum interstory drift and top acceleration with respect to input frequency of the sine wave corresponding to the critical double impulse with constant acceleration amplitude for three hysteretic damper stiffness ratios α = 1, 2, 3. The vertical solid line indicates the frequency calculated from the timing of the second impulse corresponding to zero restoring force in the unloading path after the first impulse. **Figure 4** presents the maximum interstory drift and top acceleration with respect to input frequency of the sine wave corresponding to the critical double impulse with constant velocity amplitude for three hysteretic damper stiffness ratios α = 1, 2, 3. As in **Figure 3**, the vertical solid line indicates the frequency calculated from the timing of the second impulse corresponding to zero restoring force in the unloading path after the first impulse. **Figure 5** illustrates the top relative acceleration with respect to input frequency of the sine wave corresponding to the critical double impulse with constant velocity amplitude for three hysteretic damper stiffness ratios α = 1, 2, 3. Although the absolute acceleration is important in the earthquake resistant design, the relative acceleration coincides with the absolute acceleration under the double impulse except at the time of input of impulses. As in **Figures 3**, **4**, the vertical solid line indicates the frequency calculated from the timing of the second impulse corresponding to zero restoring force in the unloading path after the first impulse.

Figures 3–5 demonstrate that, through the investigations on the criticality of the sine wave corresponding to the critical double impulse, the critical timing of the double impulse leads to the nonlinear resonant input frequency of the sine wave in view of the maximum interstory drift, the maximum top acceleration and the maximum relative acceleration for the constant input acceleration and the constant input velocity except for some cases.

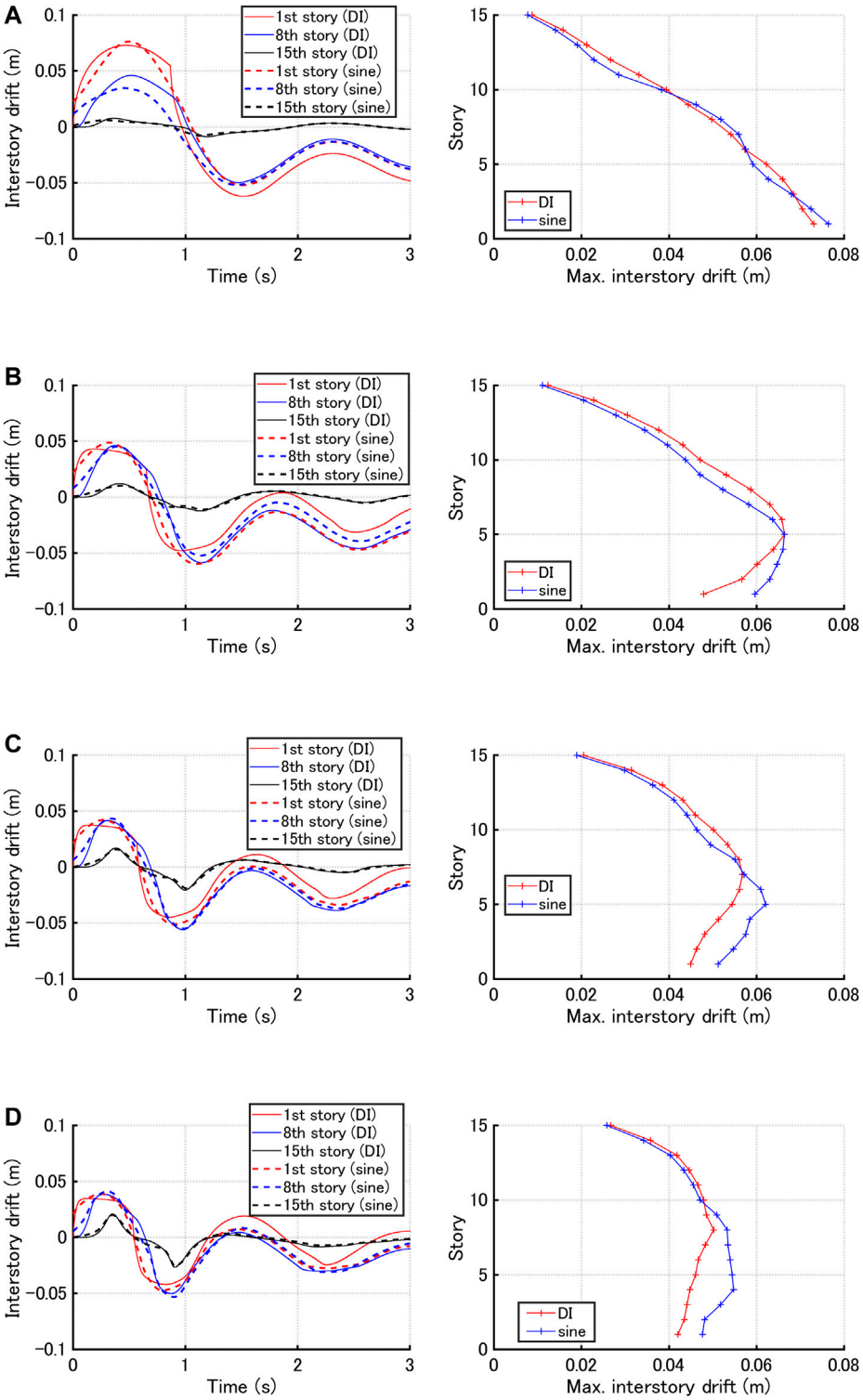

FIGURE 2 | Time histories of first, eighth and 15th-story interstory drifts and maximum interstory drift distributions of 15-story buildings with HVH system for three hysteretic damper stiffness ratios $\alpha = 0, 1, 2, 3$ under critical double impulse and corresponding sinusoidal wave, **(A)** $\alpha = 0$ (frame without hysteretic damper), **(B)** $\alpha = 1$, **(C)** $\alpha = 2$, **(D)** $\alpha = 3$.

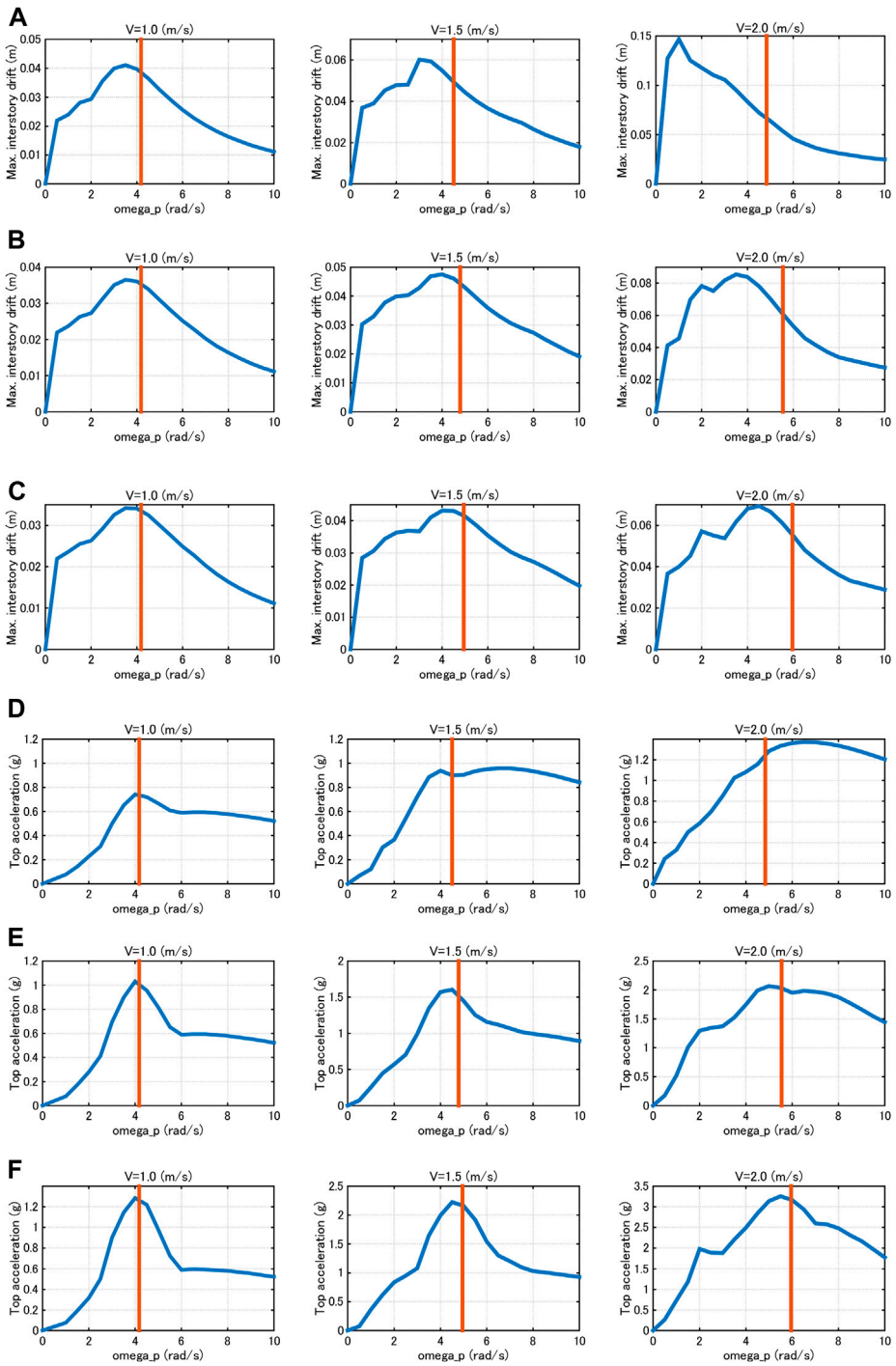

FIGURE 3 | Maximum interstory drift and top acceleration with respect to input frequency of sine wave corresponding to critical double impulse with constant acceleration amplitude, **(A)** Max. interstory drift (m): $\alpha = 1$, **(B)** Max. interstory drift (m): $\alpha = 2$, **(C)** Max. interstory drift (m): $\alpha = 3$, **(D)** Top acceleration: $\alpha = 1$, **(E)** Top acceleration: $\alpha = 2$, **(F)** Top acceleration: $\alpha = 3$.

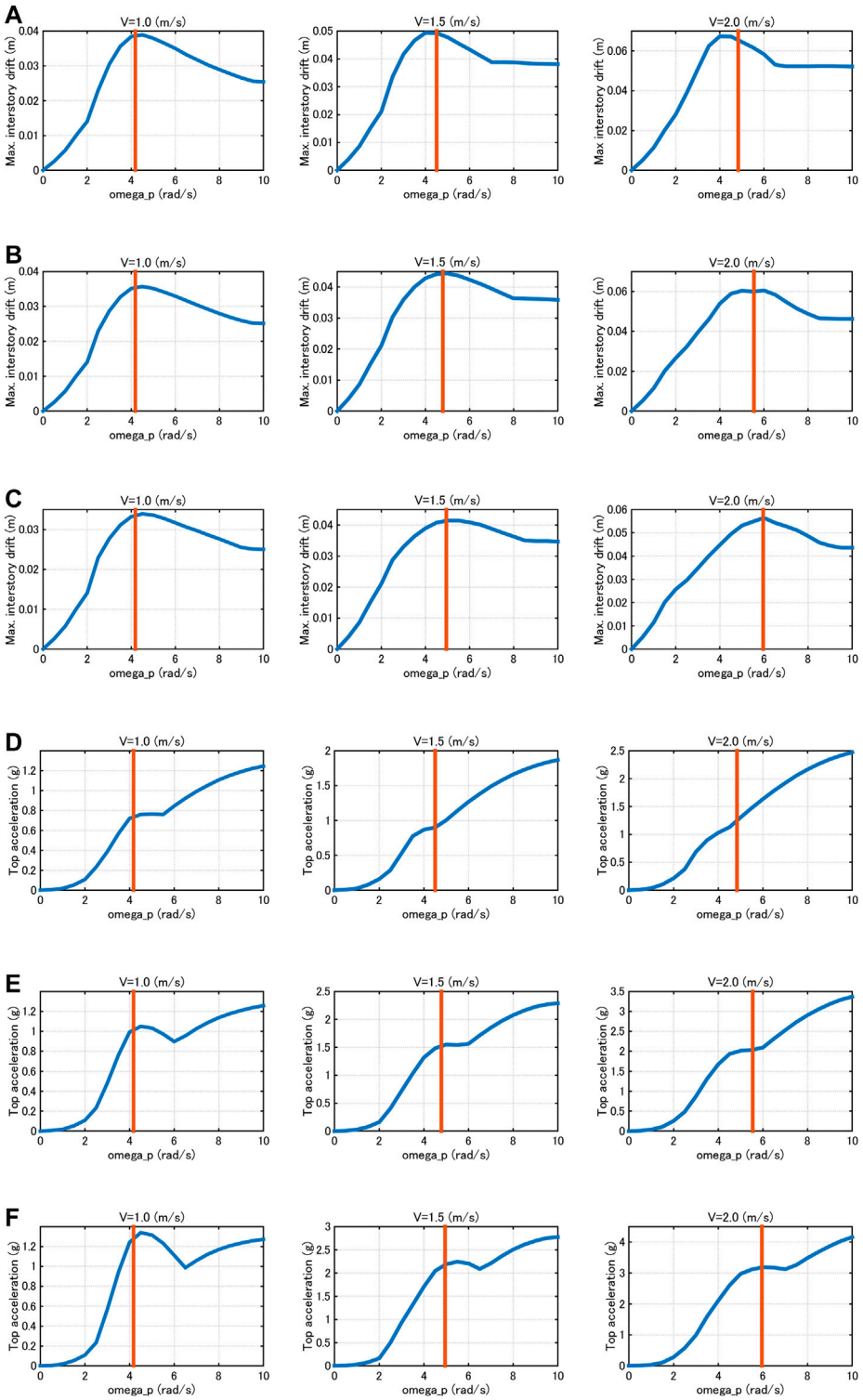

FIGURE 4 | Maximum interstory drift and top acceleration with respect to input frequency of sine wave corresponding to critical double impulse with constant velocity amplitude, **(A)** Max. interstory drift (m): $\alpha = 1$, **(B)** Max. interstory drift (m): $\alpha = 2$, **(C)** Max. interstory drift (m): $\alpha = 3$, **(D)** Top acceleration: $\alpha = 1$, **(E)** Top acceleration: $\alpha = 2$, **(F)** Top acceleration: $\alpha = 3$.

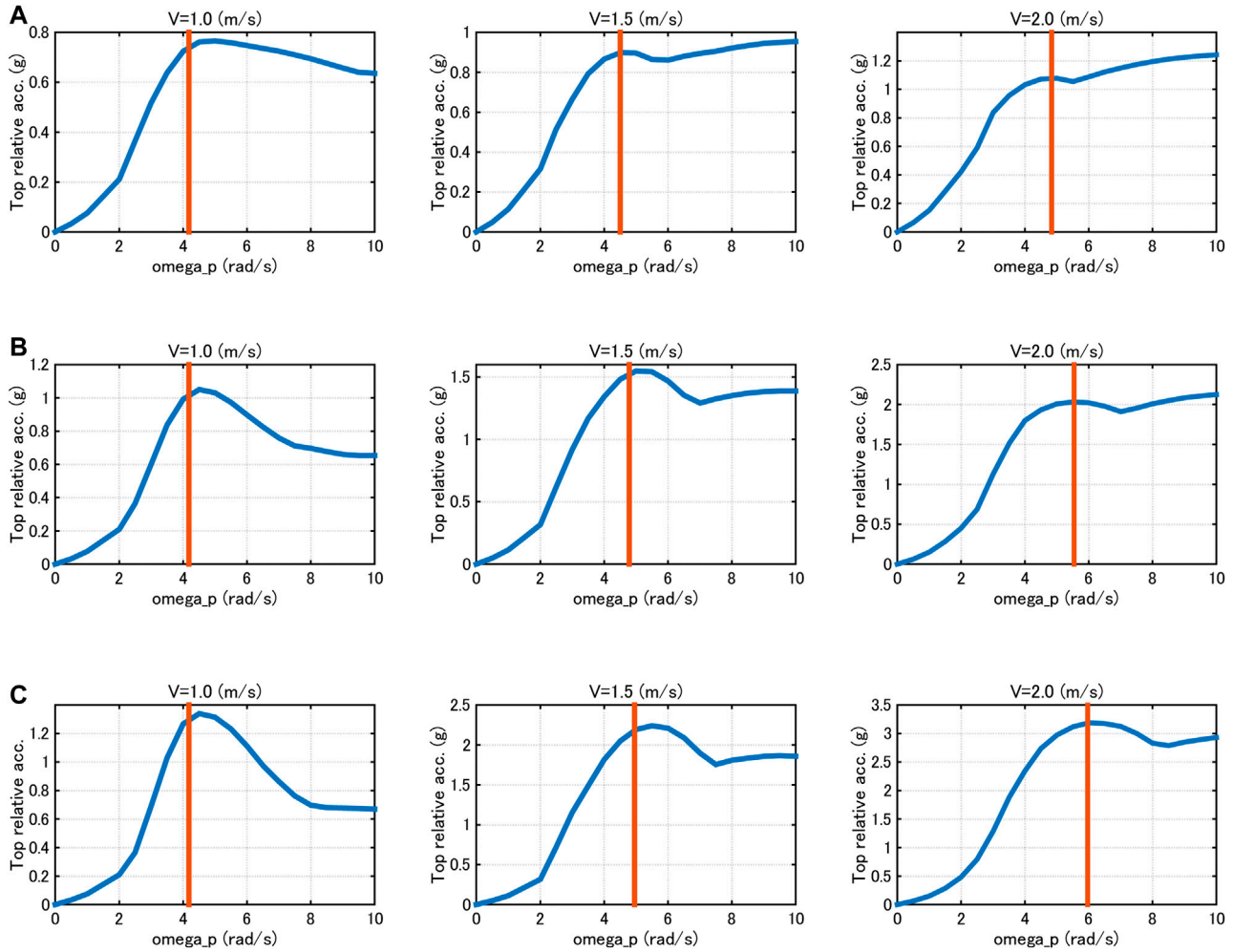

FIGURE 5 | Top relative acceleration with respect to input frequency of sine wave corresponding to critical double impulse with constant velocity amplitude, **(A)** α = 1, **(B)** α = 2, **(C)** α = 3.

OPTIMAL DESIGN OF HYSTERETIC DAMPERS WITH GAP

Stiffness Optimization

In Sections *Hysteretic-Viscous Hybrid Damper System and Responseof Frame with HVH Under Double Impulse and Corresponding Sine Wave* and *Investigation on Nonlinear Resonant Frequency of Sinusoidal Wave Transformed From Critical Double Impulse*, the response characteristics of shear building models with HVH damper systems and its nonlinear resonant frequencies were investigated. In this section, the optimal design of hysteretic dampers with gap mechanism (stiffness and gap quantity) is discussed. Since a simple setting of damper properties (common setting of damper parameters throughout all stories), stiffness ratios and gap quantities of hysteretic dampers are set commonly throughout all stories (α and d_{gh}).

First of all, the optimal stiffness of hysteretic dampers with gap mechanism is searched from the viewpoint of suppression of deformation and acceleration. The parameters except the hysteretic damper stiffness ratio α are the same as in **Table 1**.

Figure 6 shows the maximum interstory drift distributions for various hysteretic damper stiffness ratios and the story ductility factors with respect to hysteretic damper stiffness ratio for input velocity levels V = 1.0, 1.5, 2.0 (m/s) under the sine waves corresponding to the critical double impulses. It can be observed that, as the hysteretic damper stiffness ratio becomes larger, the deformation concentration in lower stories is controlled to lower levels. Furthermore, the usage of hysteretic dampers in the elastic range is effective for the control of deformation even for larger input.

Figure 7 presents the maximum acceleration distributions for various hysteretic damper stiffness ratios and the top acceleration with respect to hysteretic damper stiffness ratio for input velocity levels V = 1.0, 1.5, 2.0 (m/s) under sine waves corresponding to critical double impulses. It can be observed that, as the hysteretic damper stiffness ratio becomes larger, the acceleration

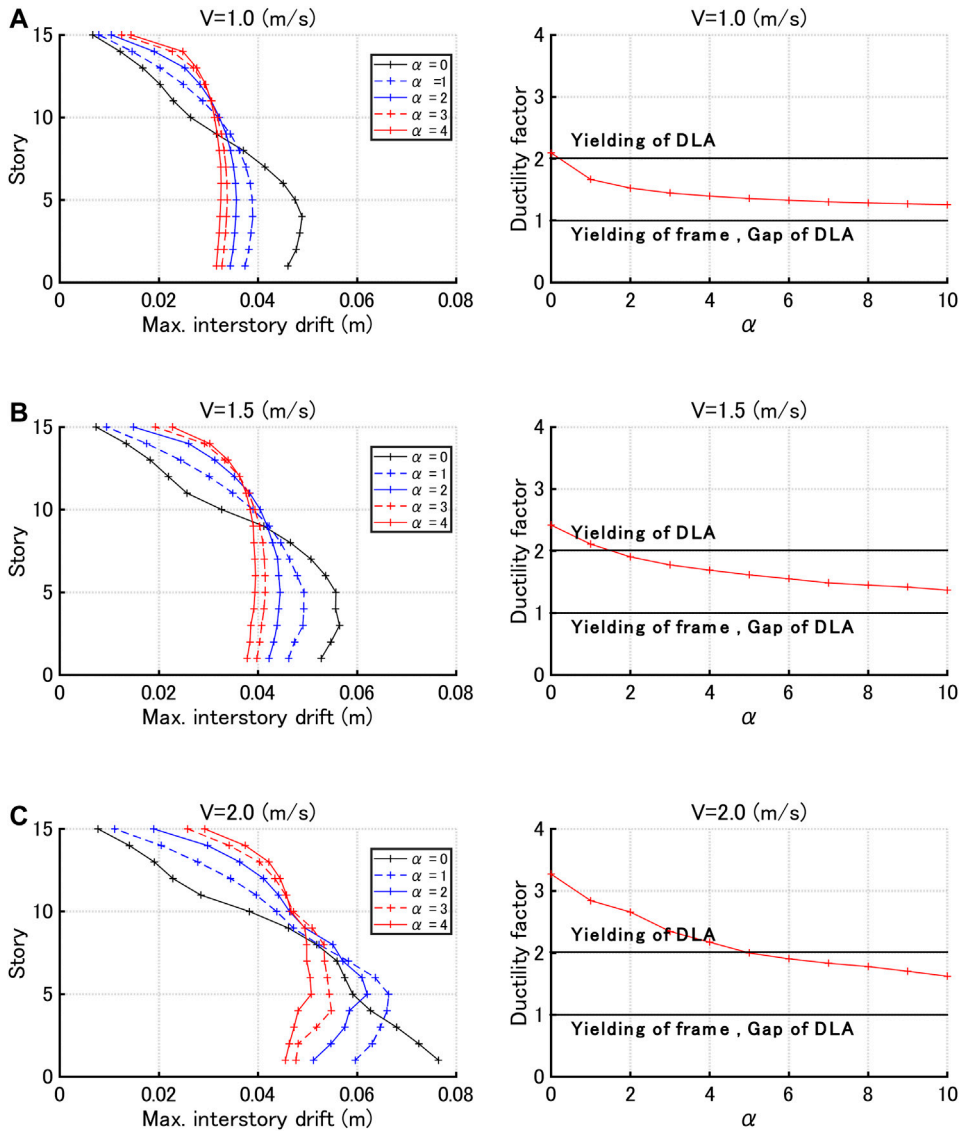

FIGURE 6 | Maximum interstory drift distributions for various hysteretic damper stiffness ratios and story ductility factor with respect to hysteretic damper stiffness ratio under sine waves corresponding to critical double impulses with three input velocity levels, **(A)** V = 1.0 (m/s), **(B)** V = 1.5 (m/s), **(C)** V = 2.0 (m/s).

distributions become extremely large. This indicates that a compromise of the maximum interstory drift and the maximum acceleration should be considered by selecting an appropriate hysteretic damper stiffness ratio.

Figure 8 shows the following three parameters x_1, x_2, x_3 with respect to hysteretic damper stiffness ratio for three input velocity levels V = 1.0, 1.5, 2.0 (m/s).

$$x_1 = d_{\max}/d_y + a_{\max}/20, \tag{11}$$

$$x_2 = d_{\max}/d_y + a_{\max}/30, \tag{12}$$

$$x_3 = d_{\max}/d_y + a_{\max}/40, \tag{13}$$

where $d_{\max}$ is the maximum interstory drift and $a_{\max}$ is the maximum acceleration. The numbers 20, 30, 40 (m/s) in the denominator of the second terms indicate the parameters for normalization of the top acceleration in relation to the normalized maximum interstory drift. It can be understood that, as this number becomes larger, the deformation index is weighted strongly. On the other hand, as this number becomes smaller, the acceleration index is weighted strongly. From **Figure 8**, it can be drawn that, while a rather small hysteretic damper stiffness ratio exhibits an optimal value in x_1 (acceleration is treated as a principal index), a larger hysteretic damper stiffness ratio exhibits an optimal value in x_3 (deformation is treated as a principal index).

Gap Quantity Optimization

In this section, the gap quantity optimization is conducted. The parameters except the gap quantity d_{gh} are the same as in **Table 1**.

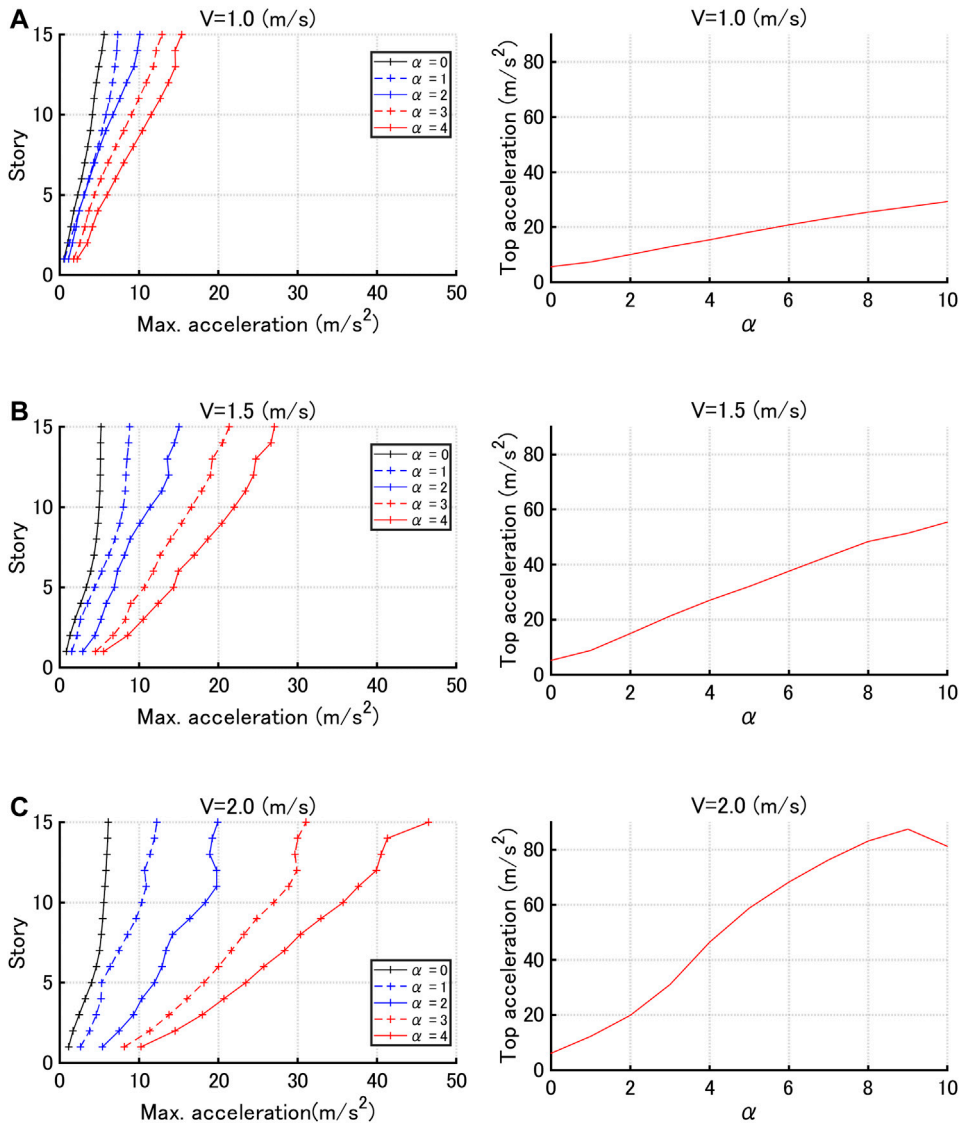

FIGURE 7 | Maximum acceleration distributions for various hysteretic damper stiffness ratios and top acceleration with respect to hysteretic damper stiffness ratio under sine waves corresponding to critical double impulses with three input velocity levels, **(A)** V = 1.0 (m/s), **(B)** V = 1.5 (m/s), **(C)** V = 2.0 (m/s).

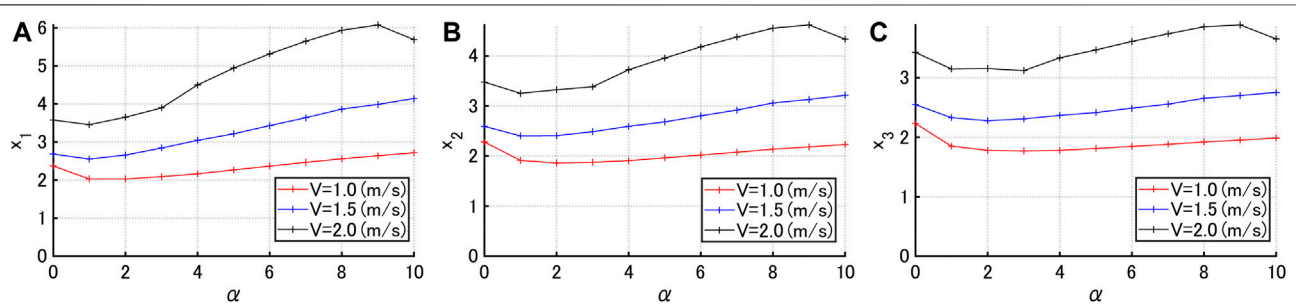

FIGURE 8 | Indices x_1, x_2, x_3 in terms of maximum interstory drift and top acceleration with respect to hysteretic damper stiffness ratio α for three input velocity levels V = 1.0, 1.5, 2.0 (m/s), **(A)** x_1, **(B)** x_2, **(C)** x_3.

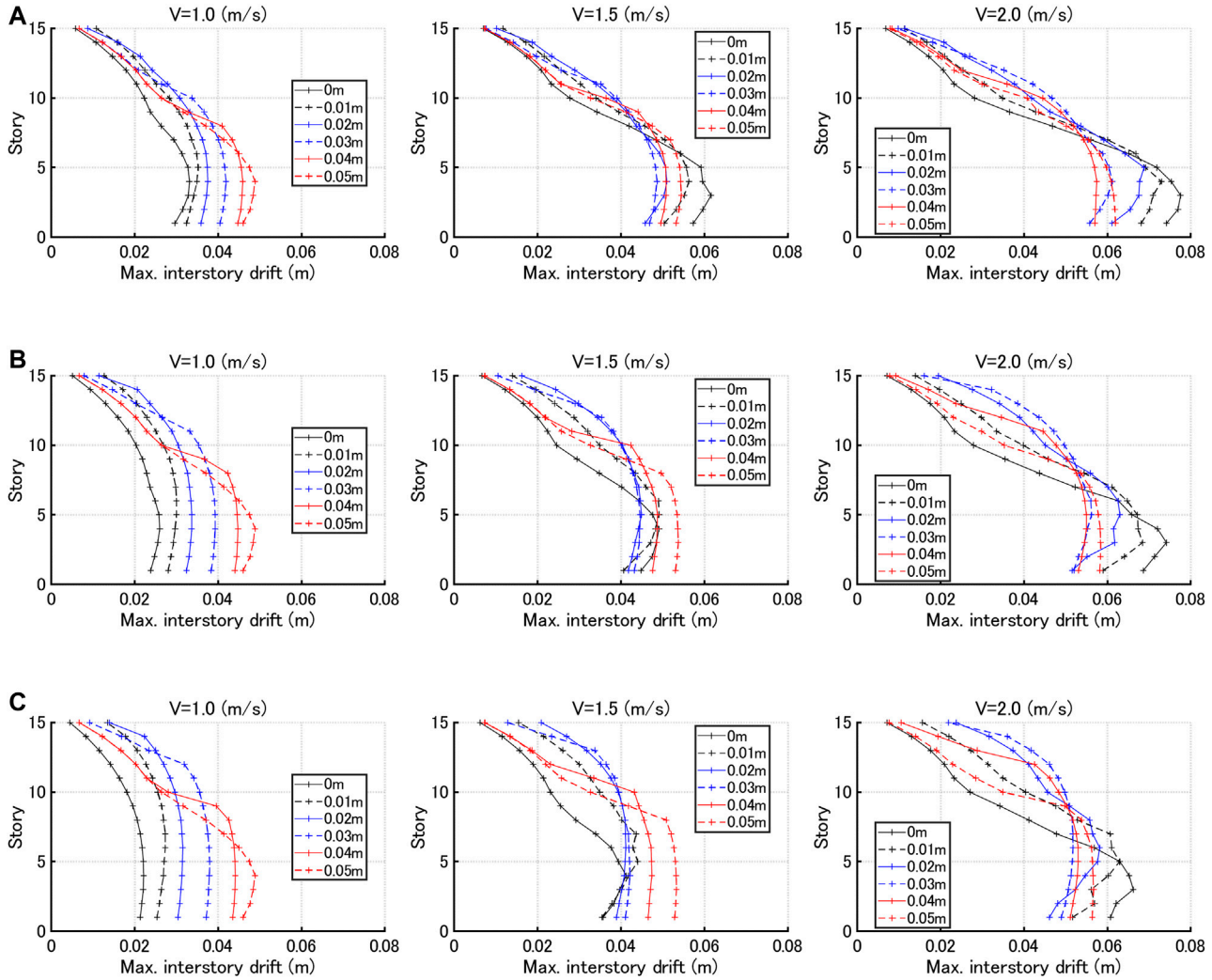

FIGURE 9 | Maximum interstory drift distributions for various gap quantities and three hysteretic damper stiffness ratios under sine waves corresponding to critical double impulses, **(A)** Hysteretic damper stiffness ratio $\alpha = 1$, **(B)** $\alpha = 2$, **(C)** $\alpha = 3$.

Figure 9 shows the maximum interstory drift distributions for various gap quantities under sine waves corresponding to the critical double impulses with three input velocity levels $V = 1.0$, 1.5, 2.0 (m/s). It can be observed from **Figure 9** that, when the input velocity level is small, the maximum interstory drifts in lower stories become larger for the increasing trigger level of hysteretic dampers (gap quantity) irrespective of α. On the other hand, when the input velocity level is large, the maximum interstory drifts in lower stories become smaller for the increasing trigger level of hysteretic dampers (gap quantity) irrespective of α. Furthermore, it can be found that, when the input velocity level becomes larger, the maximum interstory drift exhibits the smallest value for a certain value of gap quantity. This means that the case of the working of hysteretic dampers after the reduction of velocities in building frames is more effective for decreasing the maximum interstory drift than the case of the working of hysteretic dampers just after the input of the sine wave. In addition, the reason why the maximum interstory drift becomes larger for the increasing gap quantity is due to the fact that the working of hysteretic dampers becomes later and hysteretic dampers cannot suppress the maximum interstory drifts. From these results, it can be concluded that, although the decreasing of gap quantity and the faster working of hysteretic dampers just after the input of the sine wave are effective for decreasing the maximum interstory drift, it may become larger when the building frame velocity at the working of hysteretic dampers is excessively large.

Figure 10 presents the maximum interstory drift with respect to gap quantity for three input velocity levels $V = 1.0$, 1.5, 2.0 (m/s). The dotted line indicates the frame yield level. It can be observed that the response exhibits a constant value for the gap larger than a certain value. This is because the maximum interstory drift is smaller than the trigger level of hysteretic dampers (gap quantity) and the hysteretic dampers do not work.

Figure 11 illustrates the maximum acceleration distributions for various gap quantities under sine waves corresponding to the

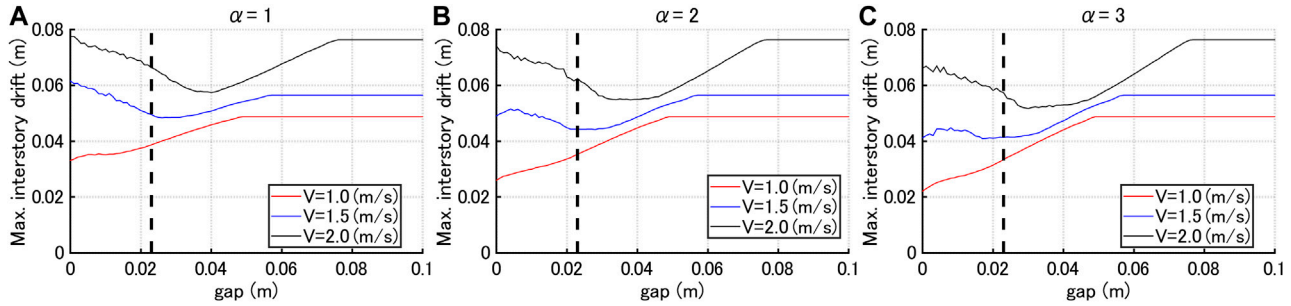

FIGURE 10 | Maximum interstory drift with respect to gap quantity for three input velocity levels V = 1.0, 1.5, 2.0 (m/s) and three hysteretic damper stiffness ratios, **(A)** α = 1, **(B)** α = 2, **(C)** α = 3.

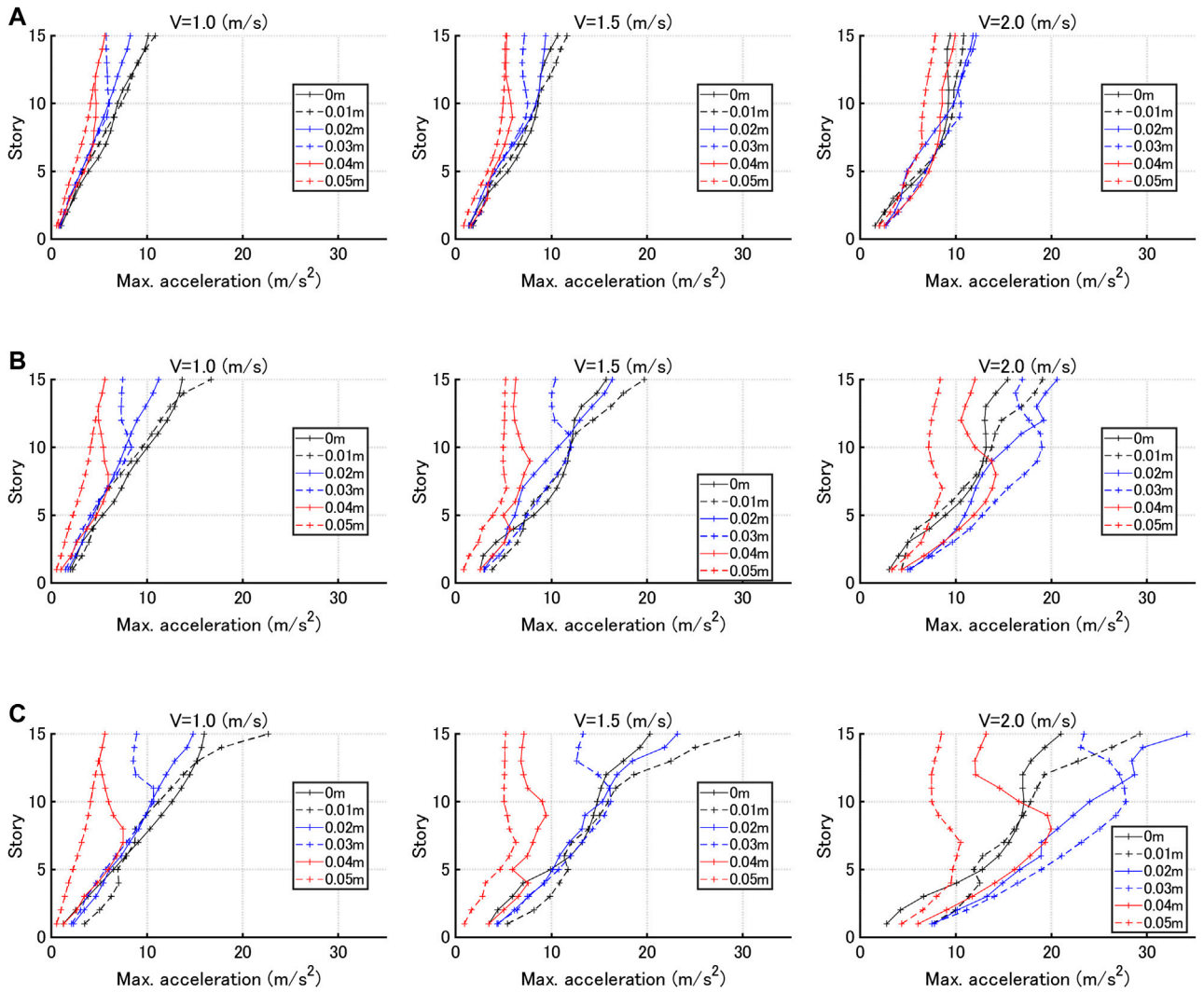

FIGURE 11 | Maximum acceleration distributions for various gap quantities under sine waves corresponding to critical double impulses, **(A)** α = 1, **(B)** α = 2, **(C)** α = 3.

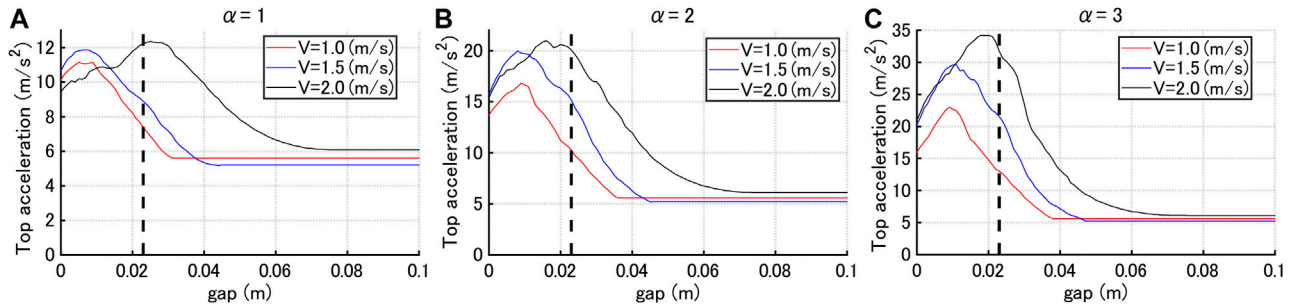

FIGURE 12 | Top acceleration with respect to gap quantity for three input velocity levels V = 1.0, 1.5, 2.0 (m/s) and three hysteretic damper stiffness ratios, **(A)** α = 1, **(B)** α = 2, **(C)** α = 3.

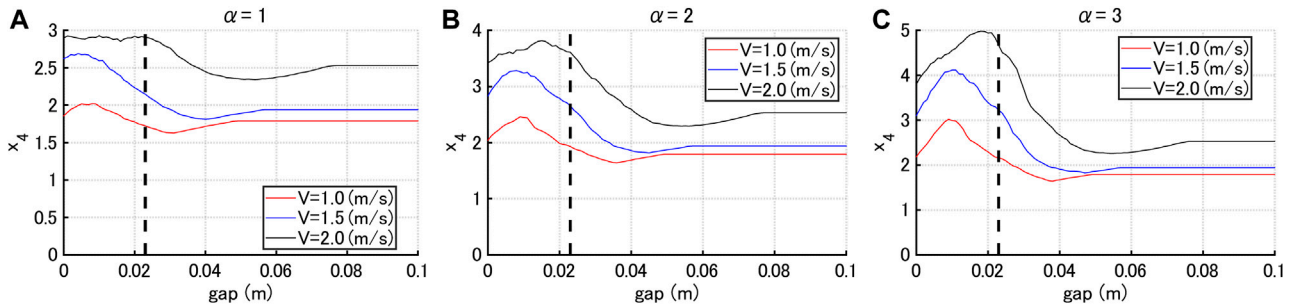

FIGURE 13 | Index x_4 in terms of maximum interstory drift and top acceleration with respect to gap quantity for three input velocity levels V = 1.0, 1.5, 2.0 (m/s) and three hysteretic damper stiffness ratios, **(A)** α = 1, **(B)** α = 2, **(C)** α = 3.

critical double impulses with three input velocity levels V = 1.0, 1.5, 2.0 (m/s). It can be observed from **Figure 11** that, while the maximum accelerations in lower stories do not change so much for variable gap quantity, those in upper stories are much affected and become smaller as the gap quantity becomes larger.

Figure 12 shows the top acceleration with respect to gap quantity for three input velocity levels V = 1.0, 1.5, 2.0 (m/s). The dotted line indicates the frame yield level. It can be observed that the acceleration response exhibits a constant value for the gap larger than a certain value. This is because the maximum interstory drift is smaller than the trigger level of hysteretic dampers (gap quantity) and the hysteretic dampers do not work. Furthermore, it is found that, as the gap quantity becomes larger, the top acceleration exhibits a local maximum. From these results, it can be concluded that, when the frame velocity at the working of hysteretic dampers is large, the maximum acceleration becomes large. In addition, it is suggested that the worst selection of the gap quantity giving the maximum acceleration should be avoided.

Consider the following parameter x_4 in terms of the maximum interstory drift and top acceleration.

$$x_4 = d_{\max}/0.04 + a_{\max}/9.8, \tag{14}$$

where $d_{\max}$ is the maximum interstory drift and $a_{\max}$ is the maximum acceleration as defined above. The number 9.8 (m/s) in the denominator of the second term indicates the parameter for normalization of the top acceleration in relation to the maximum interstory drift normalized by the deformation parameter 0.04 (m) (1/100 of story height).

Figure 13 presents the index x_4 in terms of the maximum interstory drift and top acceleration for three input velocity levels V = 1.0, 1.5, 2.0 (m/s) and three hysteretic damper stiffness ratios α = 1, 2, 3. It can be observed from **Figure 13** that the gap

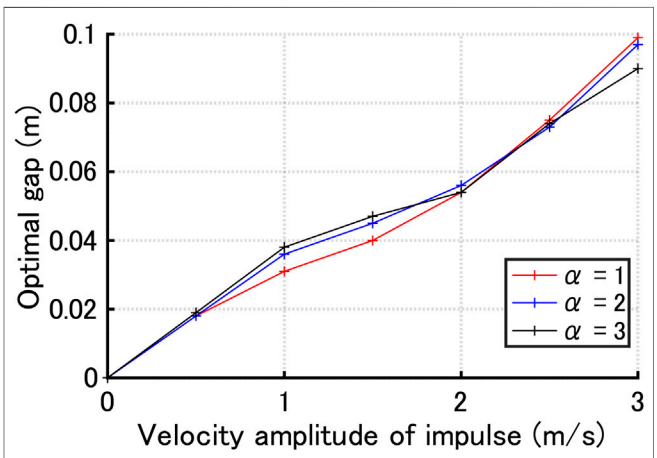

FIGURE 14 | Optimal gap quantity vs. input velocity level of critical double impulse for three hysteretic damper stiffness ratios α = 1, 2, 3.

quantity minimizing the index x_4 in terms of the maximum interstory drift and the top acceleration exists for various input velocity levels and various hysteretic damper stiffness ratios. In other words, the index in terms of the maximum interstory drift and the maximum acceleration can be used as an appropriate parameter for deriving the optimally compromised gap quantity of hysteretic dampers with gap mechanism for various input velocity levels and various hysteretic damper stiffness ratios. In more detail, when the input velocity level is small, the index x_4 exhibits the minimum around gap quantity = 0.03 (m) and, when the input velocity level is large, the index x_4 exhibits the minimum around gap quantity = 0.05 (m).

Figure 14 demonstrates that the optimal gap quantity vs. input velocity level of the critical double impulse can be derived for various hysteretic damper stiffness ratios. It can be observed that the optimal gap quantity attains almost the same value for the input velocity level independent of α in the range of $\alpha = 1 \sim 3$. Furthermore, the optimal gap quantity varies approximately linearly for the input velocity level and it becomes large according to the increase of the input velocity level.

Other Parameter Optimization

The investigation on the effect of damping coefficients of viscous dampers in the HVH control system was conducted in the previous paper (Hashizume and Takewaki, 2020b), although only the maximum interstory drifts were treated as the response parameters. It was concluded that the increase of the damping quantity of viscous dampers is effective for the suppression of the maximum interstory drifts. On the other hand, the yielding displacements (without gap quantity) of hysteretic dampers were not investigated because a fixed-type hysteretic damper is assumed to be used. However, it was pointed out that the design of hysteretic dampers so as to attain just the yield point when the frame reaches the maximum interstory drifts is a preferable design leading to the minimum interstory drift.

Response to Pulse-Type Recorded Ground Motion With Large Amplitude

It seems important to investigate the response to pulse-type recorded ground motions with large amplitude. This investigation was conducted in the previous paper (Hashizume and Takewaki, 2020b), although only the maximum interstory drifts were treated as the response parameters. It was demonstrated that the HVH control system is effective also for pulse-type recorded ground motions with large amplitude. However, it should be remarked that, while only the critical resonant response was dealt with in the double impulse pushover (DIP) analysis, the analysis to recorded ground motions does not necessarily provide the worst scenario. The DIP analysis was proposed by Akehashi and Takewaki (2019). The range of the velocity amplitude of the double impulse is assumed. Then the response to the critical double impulse with the initial velocity amplitude (the smallest one) is computed. This procedure is repeated for various velocity-amplitudes of the double impulse in the assumed range. The plot of the maximum interstory drift with respect to the velocity-amplitude of the double impulse indicates the result of the DIP analysis.

The research on the response characteristics for a broader class of pulse-type recorded ground motions is desired in the future.

CONCLUSION

The viscous-hysteretic hybrid (HVH) damper system proposed by one of the present authors (Hashizume and Takewaki, 2020b) has a property that, when the hysteretic dampers with gap mechanism become active (stiffness starts working), the acceleration of building frames with this damper system exhibits large values in spite of the advantageous feature to prevent excessive deformation. It is therefore desired that the maximum interstory drift and the maximum acceleration exhibit reasonable values with appropriate compromise. The following conclusions were derived.

(1) The double impulse can simulate the maximum interstory drifts properly under a sine wave as a representative of the main part of near-field ground motions. However, it cannot simulate the maximum accelerations due to its impulsive nature. In this case, the sine wave corresponding to the double impulse can play an important role in the simulation of the maximum accelerations. Even in such circumstance, the analysis using the double impulse is important because it can obtain the critical timing of the double impulse, i.e. the nonlinear resonant frequency of the sine wave.
(2) The investigations on the criticality of the sine wave corresponding to the critical double impulse showed that the critical timing of the double impulse leads to the nonlinear resonant frequency of the sine wave in view of the maximum interstory drift except for some cases. A similar property on the criticality was also demonstrated for the maximum top acceleration and the maximum relative acceleration for the constant input acceleration and the constant input velocity.
(3) The index x_4 in terms of the maximum interstory drift and the maximum acceleration can be used as an appropriate parameter for deriving the optimally compromised gap quantity of hysteretic dampers with gap mechanism for various input velocity levels and various hysteretic damper stiffness ratios.
(4) The relation of the optimal gap quantity with the input velocity level of the critical double impulse can be derived for various hysteretic damper stiffness ratios. It was confirmed that this relation is approximately independent of the hysteretic damper stiffness ratio.

DATA AVAILABILITY STATEMENT

The raw data supporting the conclusions of this article will be made available by the authors, without undue reservation.

AUTHOR CONTRIBUTIONS

SI formulated the problem, conducted the computation, and wrote the paper. IT supervised the research and wrote the paper.

FUNDING

Part of the present work is supported by the Grant-in-Aid for Scientific Research (KAKENHI) of Japan Society for the Promotion of Science (No.18H01584). This support is greatly appreciated.

REFERENCES

Adachi, F., Yoshitomi, S., Tsuji, M., and Takewaki, I. (2013). Nonlinear optimal oil damper design in seismically controlled multi-story building frame. *Soil Dyn. Earthq. Eng.* 44 (1), 1–13. doi:10.1016/j.soildyn.2012.08.010

Aiken, I. D., Nims, D. K., Whittaker, A. S., and Kelly, J. M. (1993). Testing of passive energy dissipation systems. *Earthq. Spectra* 9, 335–370. doi:10.1193/1.1585720

Akehashi, H., and Takewaki, I. (2019). Optimal viscous damper placement for elastic-plastic MDOF structures under critical double impulse. *Front. Built Environ.* 5, 20. doi:10.3389/fbuil.2019.00020

Akehashi, H., Kojima, K., and Takewaki, I. (2018). Critical response of SDOF damped bilinear hysteretic system under double impulse as substitute for near-fault ground motion. *Front. Built Environ.* 4, 5. doi:10.3389/fbuil.2018.00005

Attard, T. L. (2007). Controlling all interstory displacements in highly nonlinear steel buildings using optimal viscous damping. *J. Struct. Eng.* 133 (9), 1331–1340. doi:10.1061/(asce)0733-9445(2007)133:9(1331)

Aydin, E., Boduroglub, M. H., and Guney, D. (2007). Optimal damper distribution for seismic rehabilitation of planar building structures. *Eng. Struct.* 29, 176–185. doi:10.1016/j.engstruct.2006.04.016

Bruneau, M., Chang, S. E., Eguchi, R. T., Lee, G. C., O'Rourke, T. D., Reinhorn, A. M., et al. (2003). A framework to quantitatively assess and enhance the seismic resilience of communities. *Earthq. Spectra* 19 (4), 733–752. doi:10.1193/1.1623497

Cimellaro, G., Reinhorn, A., and Bruneau, M. (2010). Framework for analytical quantification of disaster resilience. *Eng. Struct.* 32 (11), 3639–3649. doi:10.1016/j.engstruct.2010.08.008

De Domenico, D., and Ricciardi, G. (2019). Earthquake protection of structures with nonlinear viscous dampers optimized through an energy-based stochastic approach. *Eng. Struct.* 179, 523–539. doi:10.1016/j.engstruct.2018.09.076

De Domenico, D., Ricciardi, G., and Takewaki, I. (2019). Design strategies of viscous dampers for seismic protection of building structures: a review. *Soil Dyn. Earthq. Eng.* 118, 144–165. doi:10.1016/j.soildyn.2018.12.024

Elias, S., and Matsagar, V. (2019). Seismic vulnerability of a non-linear building with distributed multiple tuned vibration absorbers. *Struct. Infrastruct. Eng.* 15 (8). doi:10.1080/15732479.2019.1602149

Hanson, R. D., and Soong, T. T. (2001). *Seismic design with supplemental energy dissipation devices*. Oakland, CA: EERI.

Hanson, R. D. (1993). Supplemental damping for improved seismic performance. *Earthq. Spectra* 9, 319–334. doi:10.1193/1.1585719

Hashizume, S., and Takewaki, I. (2020a). Hysteretic-viscous hybrid damper system for long-period pulse-type earthquake ground motions of large amplitude. *Front. Built Environ.* 6, 62. doi:10.3389/fbuil.2020.00062

Hashizume, S., and Takewaki, I. (2020b). Hysteretic-viscous hybrid damper system with stopper mechanism for tall buildings under earthquake ground motions of extremely large amplitude. *Front. Built Environ.* 6, 583543. doi:10.3389/fbuil.2020.583543

Kojima, K., and Takewaki, I. (2015). Critical earthquake response of elastic-plastic structures under near-fault ground motions (Part 1: fling-step input). *Front. Built Environ.* 1, 12. doi:10.3389/fbuil.2015.00012

N. Lagaros, V. Plevris, and C. C. Mitropoulou (Editors) (2013). *Design optimization of active and passive structural control systems*: Information Science Reference, Hershey, USA.

Lavan, O., and Levy, R. (2010). Performance based optimal seismic retrofitting of yielding plane frames using added viscous damping. *Earthq. Struct.* 1 (3), 307–326. doi:10.12989/eas.2010.1.3.307

Murakami, Y., Noshi, K., Fujita, K., Tsuji, M., and Takewaki, I. (2013). Optimal placement of hysteretic dampers via adaptive smoothing algorithm. *Proc. Iceas13 Asem13*, 1821–1835. doi:10.1007/978-3-319-18320-6_13

E. Noroozinejad, I. Takewaki, T.Y. Yang, A. Astaneh-Asl, and P. Gardoni (Editors) (2019). *Resilient structures and infrastructures*. Berlin, Germany: Springer.

Palermo, M., Silvestri, S., Landi, L., Gasparini, G., and Trombetti, T. (2016). Peak velocities estimation for a direct five-step design procedure of inter-storey viscous dampers. *Bull. Earthquake Eng.* 14 (2), 599–619. doi:10.1007/s10518-015-9829-8

Palermo, M., Silvestri, S., and Trombetti, T. (2017). On the peak inter-storey drift and peak inter-storey velocity profiles for frame structures. *Soil Dyn. Earthq. Eng.* 94, 18–34. doi:10.1016/j.soildyn.2016.12.009

Palermo, M., Silvestri, S., Landi, L., Gasparini, G., and Trombetti, T. (2018). A "direct five-step procedure" for the preliminary seismic design of buildings with added viscous dampers. *Eng. Struct.* 173, 933–950. doi:10.1016/j.engstruct.2018.06.103

Shiomi, T., Fujita, K., Tsuji, M., and Takewaki, I. (2016). Explicit optimal hysteretic damper design in elastic-plastic structure under double impulse as representative of near-fault ground motion. *Ijeie* 1 (1/2), 5–19. doi:10.1504/ijeie.2016.080029

Shiomi, T., Fujita, K., Tsuji, M., and Takewaki, I. (2018). Dual hysteretic damper system effective for broader class of earthquake ground motions. *Ijeie* 2 (3), 175–202. doi:10.1504/ijeie.2018.093391

Silvestri, S., Gasparini, G., and Trombetti, T. (2010). A five-step procedure for the dimensioning of viscous dampers to be inserted in building structures. *J. Earthq. Eng.* 14 (3), 417–447. doi:10.1080/13632460903093891

Soong, T. T., and Dargush, G. F. (1997). *Passive energy dissipation systems in structural engineering*. Chichester: John Wiley & Sons.

Tabara, A. M., and De Domenico, D. (2020). Nonlinear response spectrum analysis of structures equipped with nonlinear power law viscous dampers. *Eng. Struct.* 219, 110857.

Takewaki, I., Fujita, K., Yamamoto, K., and Takabatake, H. (2011). Smart passive damper control for greater building earthquake resilience in sustainable cities. *Sustainable Cities Soc.* 1 (1), 3–15. doi:10.1016/j.scs.2010.08.002

Takewaki, I. (1997). Optimal damper placement for minimum transfer functions. *Earthquake Engng. Struct. Dyn.* 26 (11), 1113–1124. doi:10.1002/(sici)1096-9845(199711)26:11<1113::aid-eqe696>3.0.co;2-x

Takewaki, I. (2009). *Building control with passive dampers: optimal performance-based design for earthquakes*. Asia, Singapore: John Wiley & Sons Ltd.

Conflict of Interest: The authors declare that the research was conducted in the absence of any commercial or financial relationships that could be construed as a potential conflict of interest.

The handling editor declared a past co-authorship with one of the authors (IT).